Development of a plug-in fuel cell electric scooter with thermally integrated storage system based on hydrogen in metal hydrides and battery pack

Paolo Di Giorgio[1,2*], *Gabriele* Scarpati[1,2], *Giovanni* Di Ilio[1,2], *Ivan* Arsie[1,2] and *Elio* Jannelli[1,2]

[1] University of Naples "Parthenope", Naples, Italy
[2] ATENA Future Technology, Naples, Italy

Abstract. The thermal management of lithium-ion batteries in hybrid electric vehicles is a key issue, since operating temperatures can greatly affect their performance and life. A hybrid energy storage system, composed by the integration of a battery pack with a metal hydride-based hydrogen storage system, might be a promising solution, since it allows to efficiently exploit the endothermic desorption process of hydrogen in metal hydrides to perform the thermal management of the battery pack. In this work, starting from a battery electric scooter, a new fuel cell/battery hybrid powertrain is designed, based on the simulation results of a vehicle dynamic model that evaluates power and energy requirements on a standard driving cycle. Thus, the design of an original hybrid energy storage system for a plug-in fuel cell electric scooter is proposed, and its prototype development is presented. To this aim, the battery pack thermal power profile is retrieved from vehicle simulation, and the integrated metal hydride tank is sized in such a way to ensure a suitable thermal management. The conceived storage solution replaces the conventional battery pack of the vehicle. This leads to a significant enhancement of the on-board gravimetric and volumetric energy densities, with clear advantages on the achievable driving range. The working principle of the novel storage system and its integration within the powertrain of the vehicle are also discussed.

1 Introduction

Improving energy efficiency and curbing CO_2 emissions are top priority issues that need to be addressed by the automotive manufactures in the pursuit of a sustainable mobility. The transportation sector is indeed one of the largest contributors of the world's fuel consumption, taking up 49% of oil resources [1]. Battery Electric Vehicles (BEVs) represent a sustainable solution for the mobility, even if the long recharge time and the high cost of the battery pack are critical issues for their diffusion [2]. The Fuel Cell Electric Vehicle (FCEV), on the other hand, is emerging as a promising solution given its potential to provide both longer range and shorter refueling time; however, the refueling infrastructure is still under development and has high investment costs [3-5]. In this context, Plug-in Fuel Cell Electric Vehicles (PFCEVs) overcome the drawbacks of the above-mentioned solutions in terms of recharging time, refueling infrastructure and driving range. As a matter of fact, PFCEVs have a moderately-sized battery, which is rechargeable at relatively low power from the electric grid, and a small size fuel cell stack which operates as a range extender. Since the average actual power demand is only a fraction of the peak power that the vehicle power unit can provide, in a PFCEV the fuel cell can be sized on the average vehicle power demand, thus providing the required energy, while the battery pack acts as a power buffer. Thus, this configuration allows to reduce the overall costs by downsizing both the fuel cell stack and the battery pack [6-10]. Moreover, the electric range of the battery can satisfy short commutes, reducing the need of a widespread diffusion of hydrogen refueling stations that a FCEV solution would have, with advantages on the infrastructure costs [11].

The thermal management system of the battery pack is a key element for hybrid electric vehicles, and especially for PFCEVs, since in these vehicles the battery pack undergoes more severe thermal stresses than in BEVs. In fact, in PFCEVs the battery pack typically experiences higher C-rates than in BEVs, which lead to a larger heat production. Moreover, the limited size and thermal capacity of the battery pack can further worsen the thermal management issues [12]. In particular, if the temperature in a battery cell (especially if aged) rises above 80°C, the thermal runaway can be triggered and its propagation within the pack can further result in catastrophic hazards [13]. Therefore, in these vehicles, high power battery cells (with relatively low internal resistance) and an efficient thermal management system are required.

To address this critical issue, an interesting option may be represented by the use of an integrated system which combines a metal hydride (MH) hydrogen storage with a battery pack, into a single, compact, device. The

* Corresponding author: paolo.digiorgio@uniparthenope.it

idea behind this solution is to exploit the endothermic desorption process of hydrogen in metal hydrides during vehicle operation to remove the excess heat from the battery pack. In fact, by means of an ad-hoc design, the MH tank and the battery pack can be placed in direct contact to each other, thus favouring a purely conductive heat transfer between them. At the same time, the on-board energy density of the storage system of the vehicle is enhanced, since a thermal management system is not required. In this study, a specific design configuration of such a Hybrid Energy Storage System (HESS) for a plug-in fuel cell electric scooter (Fig. 1) is developed and a prototype is presented. Also, its integration within the vehicle power-unit is discussed.

Fig. 1. The plug-in fuel cell electric scooter.

The overview of this work is as follows: the study starts with the design of a fuel cell/battery hybrid powertrain for a two-wheeler. To this aim, a vehicle dynamic model is setup and used to estimate power and energy requirements. The numerical model, along with a rule-based energy management strategy, is then used to simulate the vehicle performance in typical operating conditions and to estimate the thermal power produced by the battery pack. This is used to size the MH tank integrated into the HESS. Finally, the energy performances of the proposed storage solution, in terms of gravimetric and volumetric energy densities, are evaluated and compared to those for the conventional battery pack of the base plug-in fuel cell electric scooter configuration.

2 Plug-in fuel cell electric scooter architecture

The base vehicle is a battery electric scooter equipped with a 48V-2kW brushless DC electric motor and a 40Ah-48V lead-acid battery pack (four 12V modules connected in series). The vehicle does not enable kinetic energy recovery from braking. In the base plug-in fuel cell electric configuration of the vehicle, the lead-acid battery pack has been replaced by a more compact and performing 20Ah-48V lithium iron phosphate ($LiFePO_4$) battery pack, a Proton-Exchange Membrane (PEM) fuel cell stack and a MH tank for hydrogen storage. The fuel cell vehicle architecture keeps the same electric motor of the original vehicle. The plug-in fuel cell electric scooter was further upgraded by replacing the $LiFePO_4$ battery pack with a HESS, which is composed by a new battery pack thermally integrated with a secondary MH tank. The schematic layout of the two-wheeler powertrain configuration with the integrated HESS is shown in Fig. 2. The specific HESS design allows to downsize the battery pack, thus increasing the overall on-board energy density, as well as the hydrogen availability.

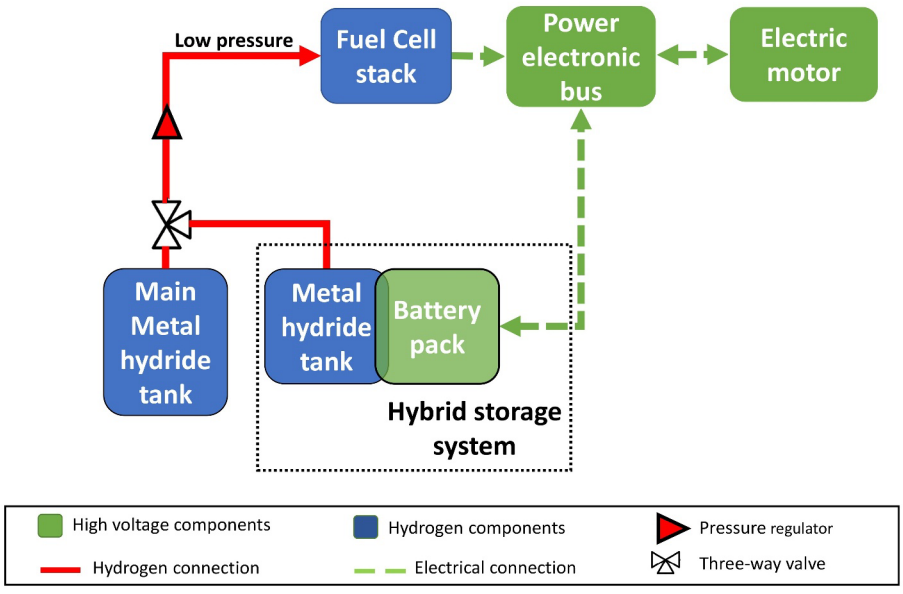

Fig. 2. Power unit and hydrogen storage system architecture for the plug-in fuel cell electric scooter.

The main MH tank is heated up by the waste heat of the fuel cell stack. The two MH tanks, are directly connected to each other by means of a three-way valve. The connection between the two tanks allows for an efficient and self-sustained thermal management of the battery pack. In fact, as shown in [14], the reaction rate for hydrogen desorption is proportional to the difference between the hydrogen pressure in tank and the desorption equilibrium pressure of hydrogen, the latter depending on temperature. Thus, depending on the battery pack temperature, the reaction rate for hydrogen desorption in the secondary tank varies: higher temperatures correspond to higher desorption equilibrium pressures, and vice-versa. Therefore, when the battery pack temperature rises above the one of the main tank, the hydrogen desorption rate in the secondary MH tank is higher than that in the main MH tank and the cooling effect on the battery pack increases. On the contrary, when the temperature of the battery pack goes below the temperature of the main MH tank, the hydrogen desorption rate is higher in the main MH tank and the cooling effect on the battery pack is reduced, as requested. During this process, the hydrogen concentration in the two tanks decreases approximately with same rate, due to the self-regulated desorption of the hydrogen content in the metal hydride. It should be emphasized that an inherent advantage from the adoption of the proposed solution is related to the hydrogen refueling infrastructure that would be required. The two MH tanks have indeed a significant lower pressure than compressed hydrogen storage systems. This would allow, in principle, a reduction of costs for the refueling infrastructure.

3 Performance analysis

In order to design the power unit of the plug-in fuel cell electric scooter, a preliminary road-test for the original battery electric scooter was made, with the aim of estimating maximum power required by the electric motor and auxiliaries power consumption. The test provided the following values: 2 kW of maximum power demand and 36 W of average auxiliary power. Since the acquired data from the road-test could not be considered as representative of a typical/mean duty cycle for the vehicle, a dynamic model was further setup to simulate the vehicle and better characterize its performance by using a standard driving cycle. According to this model, the power at the electric motor is computed as follows:

$$P_{EM} = P_t/\eta_{EM} + P_{aux} \quad (1)$$

where $\eta_{EM} = 0.85$ is the electric motor efficiency, P_{aux} is the auxiliary power, and P_t is the traction power that, assuming the road grade equal to zero, is given by:

$$P_t = 0.5\rho v^3 A C_d + f_r mgv + \delta mav \quad (2)$$

with: $\rho = 1.2$ kg/m^3 the air density, $A = 0.7$ m^2 the vehicle frontal area, $C_d = 0.7$ the drag coefficient, $f_r = 0.01$ the rolling resistance coefficient, $m = 206$ kg the vehicle mass, g the gravity acceleration, $\delta = 1.1$ the mass factor, a the instantaneous acceleration, and v the vehicle speed. Thus, an ad-hoc modified version of the Artemis urban cycle was used to assess the scooter performances. Corrections to the original Artemis speed profile were indeed necessary in order to comply with the speed constraint of the tested vehicle. The resulting driving cycle is shown in Fig. 3.

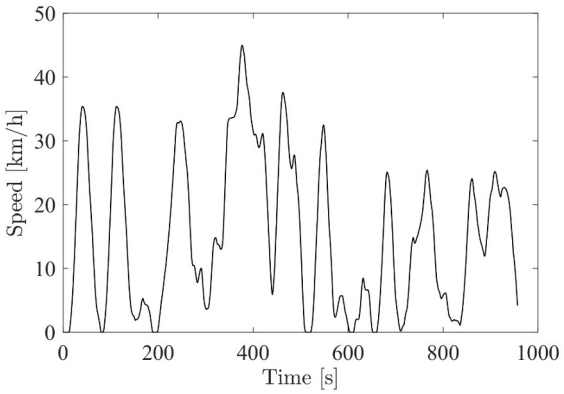

Fig. 3. Modified Artemis urban cycle, for the testing of the electric scooter performance.

The maximum and mean power obtained from the numerical model are equal to 2.8 kW and 370 W, respectively. These values have been considered to size the power unit of the new hydrogen-fueled vehicle.

4 Fuel cell design and characterization

The power unit design for the plug-in fuel cell electric scooter was made according to the following principle: the fuel cell has to be sized to provide at least the mean power requested by the electric motor, while the battery pack will satisfy the peak power requests. Therefore, a fuel cell with 1 kW of maximum power has been considered a suitable choice, since this size would allow the fuel cell to operate efficiently at values of power around the requested base load. In particular, a fuel cell system made of two Horizon FCS-C500 PEM Fuel Cell [15] modules (rated power: 500 W), connected in series, was selected. This choice leaves enough space for the main MH hydrogen storage to be placed in front of the cooling fans of the fuel cells.

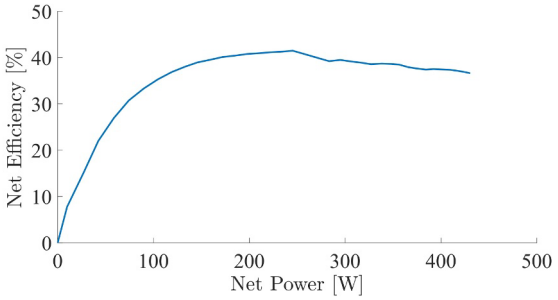

Fig. 4. Fuel cell efficiency curve.

In order to fully characterize the fuel cell performance, a bench-test was conducted: a maximum net efficiency of

40% was obtained for a value of power close to 250 W, as shown in Fig. 4.

5 Main MH tank design

The hydrogen storage in MHs is based on a reversible reaction of gaseous H_2 with a parent hydride forming metal alloy or intermetallic compound. The use of MHs allows a very high volumetric hydrogen storage density even at low pressure [16]. In addition, the endothermic nature of the MH decomposition (hydrogen desorption) results in a high inherent safety of MH-based hydrogen storage systems. The hydride material chosen for the MH tanks of the plug-in fuel cell electric scooter is the Hydralloy C5, that has been selected among commercially available room-temperature alloys. The Hydralloy C5 belongs to a class of pseudo-binary AB_2 alloys and it is produced by Gesellsclhaft für Elektrometallurgie (GfE). The hydrogen desorption characteristics of this alloy are reported in Table 1. The adopted alloy presents also a good compromise between raw material cost and hydrogen storage capacity [17].

Table 1. Hydrogen desorption characteristics of Hydralloy C5.

Parameter	Value	Ref.
Plateau pressure (@ 44 °C)	2 MPa	[18]
Max reversible H_2 content (wt %)	1.77 %	[18]
ΔH [kJ/mol$_{H2}$]	28.4	[19]
ΔS [J/(mol$_{H2}$K)]	112	[19]

In particular, the main hydrogen storage system allows to store 150g of hydrogen, and it is composed of five MyH2® SLIM 350 cartridges connected in parallel, each having a storage capacity of 30g of hydrogen. The MH cartridges are placed in front of the fuel cell fans, in order to exploit the waste heat to promote the hydrogen desorption process from the cartridges. Fig. 5 and Fig. 6 show pictures of a single MH cartridge and of a detail of the scooter prototype, where it is possible to observe the main MH tank and the fuel cell stack layout.

Fig. 5. MyH2® SLIM 350 cartridge used in the main MH tank of the plug-in fuel cell electric scooter.

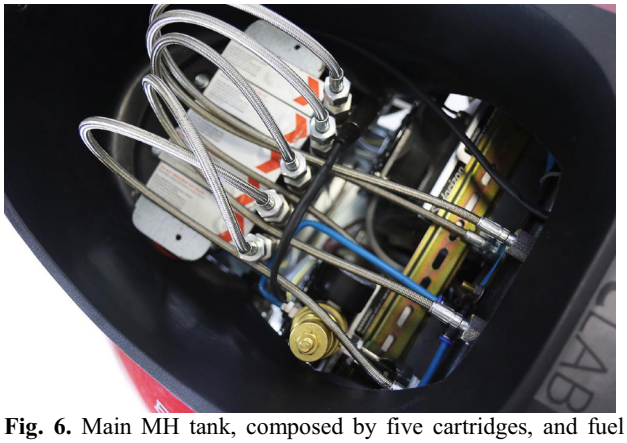

Fig. 6. Main MH tank, composed by five cartridges, and fuel cell system, on the scooter prototype.

6 Hybrid storage system design

The HESS of the new plug-in fuel cell electric scooter is composed by a battery pack integrated with a metal hydride tank. Specifically, its configuration is based on a modular hexagonal structure, shown in Fig. 7, which is used to enhance the heat transfer between the two components and increase the packing density.

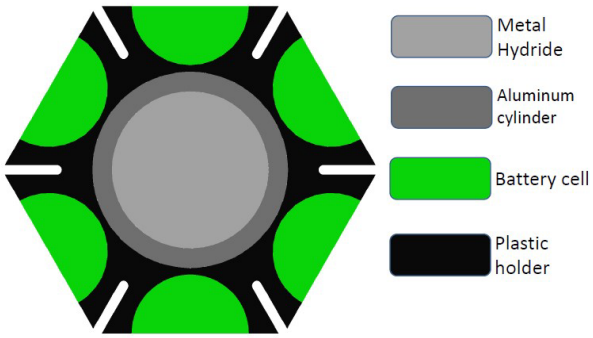

Fig. 7. 2D schematic representation of the HESS module.

In each HESS module, an aluminum cylinder containing the MH alloy is placed at the center, while six battery cells are around it. The heat transfer between the battery cells and the MH canister is purely conductive and it is ensured by a 3D-printed thermally conductive PLA holder. The reason why the holder containing battery cells and the MH canisters is made of plastic material is that it has to allow enough thermal conduction between these two components while ensuring protection to the battery cells at the same time, so to prevent spreading of thermal runway reactions. In addition, thermal insulation cavities have been included in the plastic holder between neighboring battery cells, to further reduce the risk of an undesired catastrophic thermal runaway.

In the hydrogen-fueled scooter, several hexagonal modules are combined together to form its HESS, as detailed in the following Sections.

6.1 Battery pack

The battery pack of the HESS is composed by two modules connected in series, each made of 28 Panasonic

NCR18650BD cylindrical cells (18 mm diameter, 65 mm length) in a 7s4p configuration. These are Lithium Nickel Cobalt Aluminium Oxide (NCA) cells, with 3.67 V nominal voltage and 3.2 Ah capacity. From data-sheet, these cells are able to deliver 10 A continuous discharge current, that corresponds to a C-rate of 3.125C, while the recommended charge current is 1.6 A, that is, 0.5C. The chosen battery pack configuration is designed in such a way to provide a compromise between power and energy capacity features: the overall nominal capacity of the battery pack is around 660 Wh, the maximum continuous power that it can deliver is roughly equal to 2 kW, while the maximum charging power amounts to about 330 W.

6.1.1 Battery thermal power evaluation

In order to determine the size of the integrated MH storage tank and to properly balance the HESS, the thermal power produced by the battery pack during its operation has been estimated by means of vehicle simulation. To this aim, an ad-hoc developed quasi-steady backward-looking simulator has been employed. In particular, a rule-based energy management strategy has been implemented, which consists of three different modes of operation, as follows:

- *Charge Depleting* (CD): the vehicle operates as a BEV for a battery State of Charge (SoC) higher than 60% or if the hydrogen fuel is fully depleted.

- *Charge Sustaining – constant power* (CP): the first time the battery SoC goes below 60%, and anytime the battery SoC hits the 50%, the fuel cell operates at constant power, in such a way to allow for battery partial depletion, which instead has the role of fulfilling the peak power request. In particular, the value of the fuel cell power output is set to 365 W, that, including a DC/DC efficiency of 90%, corresponds to the maximum charging power for the battery. In fact, under this mode of operation, the charging of the battery is still allowed, and it occurs anytime the overall power request is lower than the fuel cell power. Therefore, this approach allows to maximize the charging of the battery, while avoiding its damaging. The CP mode of operation is held until the SoC reaches a lower threshold value set equal to 40%.

- *Charge Sustaining – load following* (LF): whenever the battery SoC hits the lower threshold of 40%, the fuel cell operates to fully supply the electric motor and recharging the battery at the same time, that is, according to a load following mode of operation. Therefore, the fuel cell power output is made of the sum of two contributions: a constant base load equal to the CP set-point (i.e. 365 W), and a variable contribution which is equal to the electric motor power request. By this way, also this mode of operation extends battery life, since it avoids its damaging due to exceeding charging current. Clearly, the value of the power output for the fuel cell is bounded to its allowed maximum. Thus, if the electric power demand is higher than the maximum power that can be provided by the fuel cell, the request is instantaneously fulfilled by the battery.

The modified Artemis urban cycle (Fig. 3) is then used as reference driving cycle to simulate the power unit operation. The vehicle is assumed to start its journey with a battery SoC equal to 0.90. The simulation is run until the hydrogen stored on-board in the main MH tank is fully depleted and the battery SoC reaches 0.2. Fig. 8 shows the obtained battery SoC profile, with highlighted the selected power unit modes of operation.

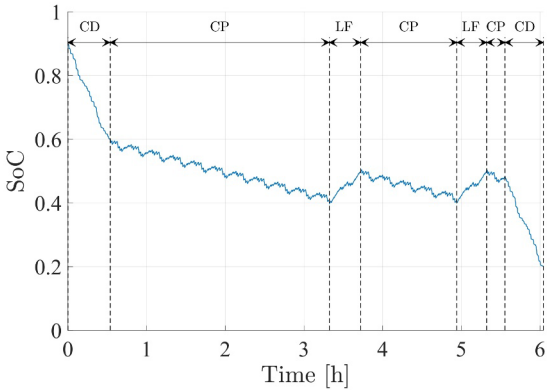

Fig. 8. Battery SoC during vehicle operation. The power unit modes of operation are reported on the top.

The driving range of the hydrogen-powered scooter –not considering the hydrogen stored into the HESS yet– is about 6 hours. The fuel cell operates near its maximum efficiency point for most of the duration of the trip, with an average efficiency of 39.5 %. Next, in Fig. 9 the fuel cell and battery power profiles are depicted against the electric motor power request, for specific time frames, corresponding to the different modes of operation, that are CD, CP and LF, respectively.

From the knowledge of the battery power output profile, the thermal power produced by each battery cell during vehicle operation has been then retrieved. To this aim, a conservative value of 55 mΩ for the battery cell overall resistance (internal resistance and connections) has been assumed. As a result, each battery cell produces on average about 0.62 W under the CD mode of operation. The battery pack heat production in charge sustaining mode is clearly lower than in CD mode. In particular, a value of 0.45 W has been obtained for the average thermal power produced per cell under the CP mode of operation, while in LF mode this value is further reduced and equal to 0.30 W since, in this case, the root mean square of the battery current is the lowest.

The thermal power produced by the battery pack must be dissipated, otherwise it can lead to an uncontrolled temperature raise which can negatively affect the battery performances and, eventually, bring to its failure. The heat removal for the battery pack of the fuel cell electric scooter is accomplished by exploiting the endothermic desorption process of hydrogen in the integrated MH tank of the HESS.

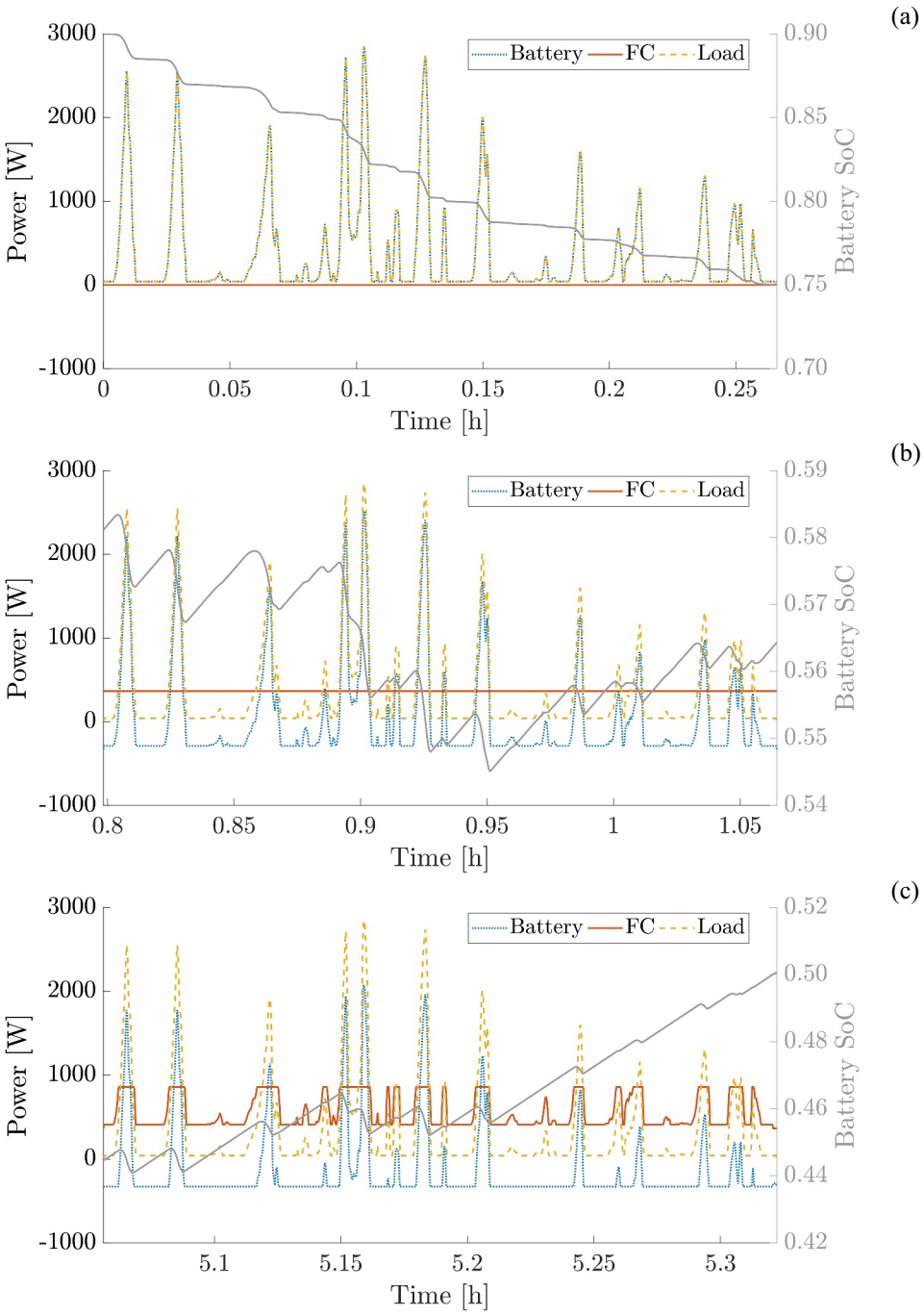

Fig. 9. Battery and fuel cell power output profiles vs the electric motor requested power, during: CD (a), CP (b) and LF (c) modes of operation. The battery SoC is also reported (grey line).

6.2 Integrated MH storage system

In order to provide an effective thermal management of the battery pack, the integrated MH tank of the HESS must be suitably designed. Therefore, the size of the cylinders containing the MH was determined taking into account the estimated amount of thermal energy produced by the battery pack during vehicle operation. Specifically, a reference cycle of 6 hours of continuous operation in CP mode (that is, the most critical condition in terms of battery thermal power production during the charge sustaining) has been assumed.

The two battery modules are stacked one on top of the other and they are crossed by seven aluminium cylinders containing the MH alloy. In Fig. 10 a prototype representation of the HESS and its components is shown.

Given the hexagonal modular geometry of the HESS, each MH cylindrical unit is surrounded by three equivalent battery cells on two rows, therefore it has to contain enough hydrogen such that its desorption ensures the thermal management of six battery cells, on average. The total heat that each MH unit must be capable of dissipating is then approximately equal to 60 kJ, according to the following equation:

$$Q = n\,\dot{Q}_b\,t \tag{3}$$

where n = 6 is the number of involved battery cells, $\dot{Q}_b$ = 0.45 W is the average thermal power produced by a single battery cell under the CP mode of operation, and t = 6 h is the assumed time of continuous operation. Such an amount of energy corresponds to the thermal energy required to desorb roughly 4.2 g of hydrogen (Table 1). By considering a maximum reversible hydrogen content of 1.77% in weight, this estimated amount of hydrogen can be reversibly stored in 232 g of metal hydride alloy, that assuming a density of the powder of about 4000 kg/m^3, is contained in about 58 cm^3. As a consequence, considering that the cylinder length is equal to 130 mm (that is, two times the battery cell height), the resulting internal diameter of each canister is around 24 mm. By setting also a 3 mm wall thickness for the aluminium cylinder (a reasonable estimate for the operating pressure range), an external diameter of 30 mm is obtained for the whole MH cylindrical unit. With this configuration, the HESS of the scooter provides an overall extra-amount of hydrogen equal to about 29 g.

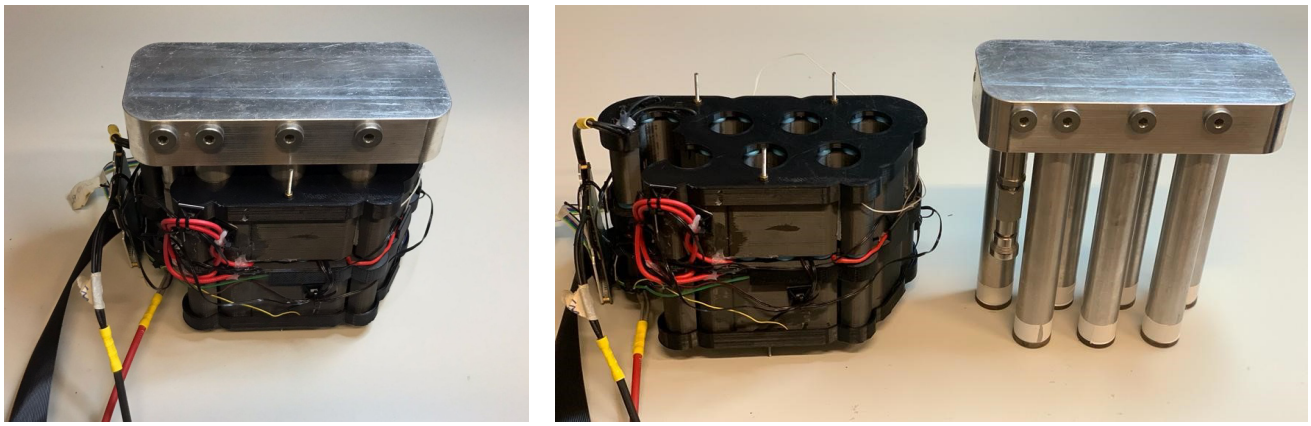

Fig. 10. HESS of the plug-in fuel cell electric scooter. Left: full system prototype. Right: detail for system components - battery pack and MH tank.

7 Energy performance

Table 2 shows the comparison between the HESS of the new plug-in fuel cell electric scooter and the battery pack of its base configuration. In particular, the values for the useful gravimetric (UED_g) and volumetric (UED_v) energy density provided in Table 2 have been calculated by assuming an 85% Depth of Discharge (DoD) for the battery pack and, in the case of HESS, by assuming an average efficiency (η_{FC}) of 50% for the fuel cell, as follows:

$$UED_g = \frac{m_{H_2} LHV_{H_2} \eta_{FC} + E_b DoD}{m_{HESS}} \quad (4)$$

$$UED_v = \frac{m_{H_2} LHV_{H_2} \eta_{FC} + E_b DoD}{V_{HESS}} \quad (5)$$

where m_{H2} is the mass of stored hydrogen, LHV_{H2} = 120 MJ/kg, E_b is the battery energy capacity, while m_{HESS} and V_{HESS} are the overall mass and volume of the HESS.

The HESS outperforms the LiFePo$_4$ battery pack solution, in terms of energy storage capabilities. In fact, the two storage systems have similar UED_g to each other but the HESS presents a significantly higher UED_v: the useful volumetric energy density of the HESS is almost the double than that of the standard battery pack. This is a key feature of the HESS, which make it particularly suitable for lightweight mobility, as in the present case, where lack of on-board space availability may represent a crucial aspect that limits the driving range.

Table 2. Main features of the HESS in comparison with the LiFePO$_4$ battery pack of the plug-in fuel cell electric scooter.

	HESS	**LiFePO$_4$ battery pack**
Overall size [mm]	90x210x240	130x160x310
Volume [L]	4.5	6.4
Weight [kg]	9	7.5
Battery pack nominal capacity [Wh]	660	960
Stored H_2 [g]	29	-
Total useful energy [kWh]	1.044	0.816
UED_g [Wh/kg]	116	109
UED_v [Wh/L]	230	127

The thermal integration of the two components, MH and battery pack, allows indeed to avoid the use of an ordinary thermal management system, in favour of additional hydrogen storage capacity. It should be also emphasized that the actual volume of the HESS is substantially lower (~3.7 L) than the one indicated in Table 2, which instead refers to the volume of the parallelepiped in which the system is inscribed, thus leading to a conservative estimation.

The overall driving range of the plug-in fuel cell electric scooter with HESS is equal to about 7 h (105 km), on the base of the reference driving cycle used in this study, while the driving range of the vehicle with

$LiFePo_4$ battery pack solution is about 6.5 h (99 km). In particular, the extra-amount of hydrogen contained in the HESS extends the range of about 1 h. In contrast, the battery electric scooter achieves 3.6 h (54 km) of driving range, under the same battery operational conditions and driving cycle.

8 Conclusions

A plug-in fuel cell electric scooter with an innovative energy storage system has been presented throughout this study. The key of such an energy storage system is the thermal coupling between a MH tank and a NCA battery pack: the two components are in direct contact to each other, thus allowing for an optimal thermal management of the system. In fact, the heat produced by the battery pack during vehicle operation is efficiently removed through the endothermic desorption process of hydrogen in the MH. Moreover, the compact design of the HESS leads to high energy density values, which in turn allow for an enhanced driving range, with respect to that achievable by the vehicle equipped with a standard battery pack. The presented solution is promising: the developed HESS prototype leaves room for further design improvement, with potential of effectively boost the performance of plug-in fuel cell lightweight vehicles.

This research was funded by the project HyLIVE – Hydrogen Light Innovative Vehicles, grant n. B63D18000430007, under the program POR Campania FESR 2014/2020.

References

1. S. Amjad, S. Neelakrishnan, R. Rudramoorthy, Renew. Sustain. Energy Rev. 14, 1104-1110 (2010)
2. E. Wood, L. Wang, J. Gonder, M. Ulsh, SAE Int. J. Commer. Veh. 6, 563-74 (2013)
3. M. Minutillo, A. Perna, P. Di Trolio, S. Di Micco, E. Jannelli, Int. J Hydrog. Energy 46, 10059-10071 (2021)
4. M. Minutillo, A. Perna, A. Forcina, S. Di Micco, E. Jannelli, Int. J Hydrog. Energy 46, 13667-13677 (2021)
5. A. Perna, M. Minutillo, S. Di Micco, P. Di Trolio, E. Jannelli, AIP Conf. Proceedings 2191, 020127 (2019)
6. P. Di Trolio, P. Di Giorgio, M. Genovese, E. Frasci, M. Minutillo, Appl. Energy 279, 115734 (2020)
7. H. Zhang, X. Li, X. Liu, J. Yan, Appl. Energy 241, 483-490 (2019)
8. G.G. Nassif, S.C.A. de Almeida, Int. J Hydrog. Energy 45, 21722-21737 (2020)
9. G. Di Ilio, P. Di Giorgio, L. Tribioli, G. Bella, E. Jannelli, Energy Convers. Manag. 243, 114423 (2021)
10. G. Di Ilio, P. Di Giorgio, L. Tribioli, V. Cigolotti, G. Bella, E. Jannelli, SAE Technical Paper 2021-09-05 (2021)
11. B. Lane, B. Shaffer, G.S. Samuelsen, Int. J. Hydrog. Energy 42, 14294-14300 (2017)
12. Q. Wang, B. Jiang, B. Li, Y. Yan, Renew. Sustain. Energy Rev. 64, 106-128 (2016)
13. H. Wang, W. Shi, F. Hu, Y. Wang, X. Hu, H. Li, Energy 224, 120072 (2021)
14. A.R. Sánchez, H.P. Klein, M. Groll, Int. J. Hydrog. Energy 28, 515-27 (2003)
15. Horizon Fuel Cell Technologies, H-500 Fuel Cell Stack User Manual (2021).
16. G. Han, Y.K. Kwon, J.B. Kim, S. Lee, J. Bae, E.A. Cho, et al., Appl. Energy 259, 114175 (2020)
17. G. Sandrock, J. Alloys Compd. 293, 877-888 (1999)
18. G. Capurso, B. Schiavo, J. Jepsen, G. Lozano, O. Metz, A. Saccone, S. De Negri, J. Bellosta von Colbe, T. Klassen, M. Dornheim, Appl. Phys. A 122, 236 (2016)
19. K. Herbrig, L. Röntzsch, C. Pohlmann, T. Weissgaerber, B. Kieback, Int. J. Hydrog. Energy 38, 7026-7036 (2013)